Journal of Alloys and Compounds 509 (2011) 10185–10189

Contents lists available at ScienceDirect

Journal of Alloys and Compounds

journal homepage: www.elsevier.com/locate/jallcom

Photoluminescence and thermoluminescence studies of $Mg_2SiO_4:Eu^{3+}$ nano phosphor

S.C. Prashantha [a], B.N. Lakshminarasappa [a,*], B.M. Nagabhushana [b]

[a] Department of Physics, Bangalore University, Bangalore 560056, India
[b] M.S. Ramaiah Institute of Technology, Bangalore 560054, India

ARTICLE INFO

Article history:
Received 18 October 2010
Received in revised form 24 March 2011
Accepted 28 March 2011
Available online 5 April 2011

Keywords:
$Mg_2SiO_4:Eu^{3+}$
Phosphor
Photoluminescence
Thermoluminescence
Optical absorption

ABSTRACT

Nanoparticles of Eu^{3+} doped Mg_2SiO_4 are prepared using low temperature solution combustion technique with metal nitrate as precursor and urea as fuel. The synthesized samples are calcined at 800 °C for 3 h. The Powder X-ray diffraction (PXRD) patterns of the sample reveled orthorhombic structure with α-phase. The crystallite size using Scherer's formula is found to be in the range 50–60 nm. The effect of Eu^{3+} on the luminescence characteristics of Mg_2SiO_4 is studied and the results are presented here. These phosphors exhibit bright red color upon excitation by 256 nm light and showed the characteristic emission of the Eu^{3+} ions. The electronic transition corresponding to $^5D_0 \rightarrow {}^7F_2$ of Eu^{3+} ions (612 nm) is stronger than the magnetic dipole transition corresponding to $^5D_0 \rightarrow {}^7F_1$ of Eu^{3+} ions (590 nm). Thermoluminescence (TL) characteristics of γ-rayed $Mg_2SiO_4:Eu^{3+}$ phosphors are studied. Two prominent and well-resolved TL glows with peaks at 202 °C and 345 °C besides a shoulder with peak at ~240 °C are observed. The trapping parameters-activation energy (E), order of kinetics (b) and frequency factor (s) are calculated using glow curve shape method and the results obtained are discussed.

1. Introduction

Long-lasting phosphors will gradually emit light at a certain wavelength with a long afterglow when they absorb energy from the ultraviolet or visible lights. This property makes long persistent phosphors, potential material to be applied in luminescent fields. In recent years, the demand for developing efficient luminescent materials such as rare earth activated powders attracted researchers because of their possible photonic applications, good luminescent characteristics, stability in high vacuum and absence of corrosive gas emission under electron bombardment when compared to currently used sulfide based phosphors. Among the rare earth ions, red-emitting trivalent europium (Eu^{3+}) is recognized as an efficient red luminescent phosphors due to its $^5D_0 \rightarrow {}^7F_{j(j=0,1,2,3,4)}$ transitions which are used in color television displays and mercury free lamps. In addition, the higher $^5D_{1,2,3}$ levels are rarely observed depending on the host lattice and the doping concentration. Efforts to enhance the luminescence nature of Eu^{3+} in host materials with low phonon energies are made. An appropriate selection of the host lattice and the suitable Eu^{3+} dopant concentration produces red emission [1–3].

Currently, nano materials and nano technology have attracted several researchers from different fields, especially from the luminescence field. Nano phosphors differ from existing bulk phosphors in terms of its electrical, optical, and structural properties. The changes in the electrical and optical characteristics of very small particles are caused by the quantum size effect, which is generated by an increase in the band gap due to a decrease in the quantum allowed state that exists in small particles, and the high surface-to-volume ratio, which improves the surface and interface effects. Rare earth and non rare earth doped inorganic phosphors are widely used in a variety of applications such as lamp industries, radiation dosimetry, color display, etc. [4,5].

Depositions of energy in a material by ionizing radiation results in generation of charge carriers (electrons or holes) and subsequently they are trapped at vacancies and interstitials. These trapped charge carriers are localized in the lattice [6]. Thermoluminescence (TL) is a powerful technique to study these charge carriers. Recent studies indicated that luminescent nano materials find potential application in dosimetry caused by ionizing radiations [7].

Over the past few years, the synthesis of inorganic nanoscale materials with specific morphologies attracted the phosphor developers. Silicate phosphors are synthesized by a variety of routes such as Solid-state reactions, Sol–Gel, Hydrothermal, Precipitation, Microwave techniques, etc. In the present studies, $Mg_2SiO_4:Eu^{3+}$ nano powders are synthesized by low temperature combustion synthesis route [LCS]. This process provides molecular level of

* Corresponding author. Tel.: +91 80 22961486. Tel.: +91 9448116281.
E-mail address: bnlnarasappa@rediffmail.com (B.N. Lakshminarasappa).

0925-8388/$ – see front matter © 2011 Elsevier B.V. All rights reserved.
doi:10.1016/j.jallcom.2011.03.148

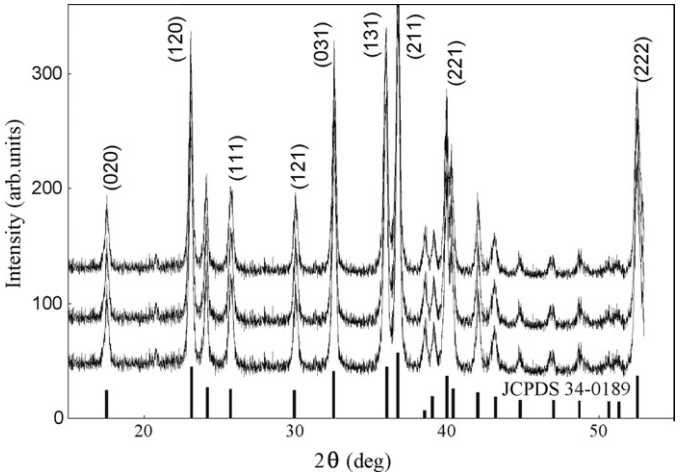

Fig. 1. XRD patterns of (a) pure (b) 3 mol% and (c) 5 mol% Eu^{3+} doped Mg_2SiO_4.

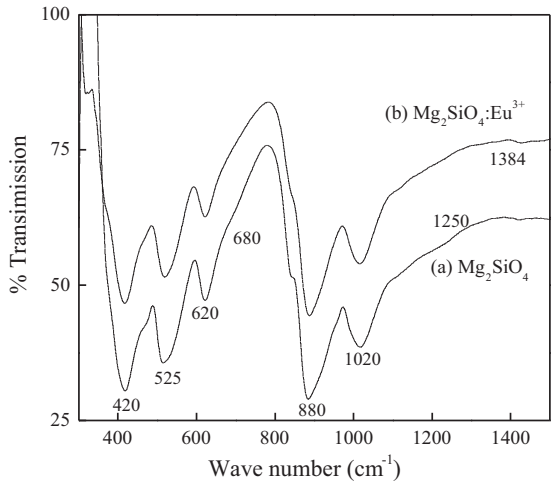

Fig. 2. FT-IR spectra of (a) pure and (b) Eu^{3+} doped Mg_2SiO_4.

mixing and high degree of homogeneity, short reaction time that leads to reduction in crystallization temperature and prevents from segregation during heating [8,9].

2. Experimental

2.1. Synthesis

Aqueous solution containing stoichiometric amounts of analar grade magnesium nitrate and urea are taken in a Petri dish of 300 ml capacity. The excess water is allowed to evaporate by heating over a hot plate until a wet powder is left out. Then the petri dish is introduced into a muffle furnace maintained at $500 \pm 10\,^{\circ}C$. The reaction mixture undergoes thermal dehydration and ignites at one spot with liberation of gaseous products such as oxides of nitrogen and carbon. The combustion propagates throughout the reaction mixture. The powder product obtained is then calcined for 800 °C for 3 h to get Enstatite ($MgSiO_3$) free Forsterite with better crystallanity and single phase.

Theoretical equation assuming complete combustion of the redox mixture used for the synthesis of Forsterite may be written as

$$4Mg(NO_3)_2 + 2SiO_2 + CO(NH_2)_2\,[\text{Urea}] \rightarrow 2\,Mg_2SiO_4 + 5\,N_2 + 12H_2O + CO_2$$

the required mole ratio of $Mg(NO_3)_2$: SiO_2: Urea is 1:0.5:0.25.

2.2. Characterization

The crystalline nature of the powder sample is characterized by PXRD using Philips X-ray diffractometer (Philips PW 1050/70, Cu Kα radiation with Ni Filter, wavelength 1.54056 Å). FTIR studies of the samples are performed with a Perkin Elmer FTIR spectrophotometer (Spectrum-1000). The optical absorption studies of the sample are made in the range 200–800 nm using Elico SL-150 spectrophotometer. Photoluminescence spectra are rerecorded with a Shimadzu Spectrofluorophotometer (RF 510) equipped with a 150 W Xenon lamp as an excitation source. Thermoluminescence glow curves are recorded using TL set up consisting of a small kanthal heating strip, temperature programmer, photomultiplier (931A), and a milivolt meter (Rishcom 100) at a heating rate of $5\,^{\circ}C\,s^{-1}$.

3. Results and discussion

Fig. 1 shows the XRD patterns of pure and Eu^{3+} doped Mg_2SiO_4 samples. The PXRD pattern of the sample is found to match exactly with those reported in the literature [10]. The average particle size (D) is estimated from the line broadening in X-ray powder using Scherrer's formula [$D = (K\lambda)/\beta\cos\theta$, where, '$K$' – constant, 'λ' – wavelength of X-rays, and 'β' – FWHM] is found to be in the range 50–60 nm [11]. All the X-ray diffraction peaks of the sample is indexed well and found single phased Mg_2SiO_4. No shift in diffraction peaks and no second phase were detected indicating that Eu^{3+} ions are obviously homogeneously mixed and effectively doped in the matrix of the host lattice in Mg^{2+} sites ($R_{Eu^{3+}} = 0.095$nm and $R_{Mg^{2+}} = 0.072$nm). From the analysis of XRD, it was revealed that the introduction of an activator (Eu^{3+}) did not influence the crystal structure of the phosphor matrix.

The room temperature infrared spectra of pure and Eu^{3+} doped Mg_2SiO_4 is recorded in the range 300–4000 cm^{-1} using KBr pellets. Fig. 2 shows the IR spectra of pure and Eu^{3+} doped magnesium silicate in the range 300–1500 cm^{-1}. The peaks at 420, 525, 620, 680, 880, 1020, 1250 and 1384 cm^{-1} are assigned to MgO_6 octahedral, Si–O, Si–O (bending), Mg–O, Si–O (stretching), (CO and Si–O), C–H and NO_3 respectively [12]. The optical absorption spectra of Mg_2SiO_4 and Mg_2SiO_4:Eu^{3+} are shown in Fig. 3. It is well established that nano scale materials have large surface to volume ratio. This results in the formation of voids on the surface as well inside the agglomerated nano particles. Such voids can cause fundamental absorption in the UV region. In addition, surfaces of nano particles are well known to comprise of several defects such as dangling bonds, regions of disorder and absorption of impurity species that result in the absorption of nano crystals. Thus, the absorption band at 250 nm may be attributed to the surface defects in nano Mg_2SiO_4:Eu^{3+} phosphor, which corresponds to oxygen to silicon (O–Si) ligand-to-metal charge-transfer (LMCT) in the SiO_3^{2-} group. The broad bands in the range 300–500 nm are attributed to the intra configurationally 4f–4f transitions from the ground $^7F_0$ level which corresponds to the excitation spectra. In case of smaller size nano particles, it is found that increase of defect distribution on the surface exhibit strong and broad absorption bands due to large surface to volume ratio [13,14]. The optical energy gap (E_g) of Eu^{3+} doped

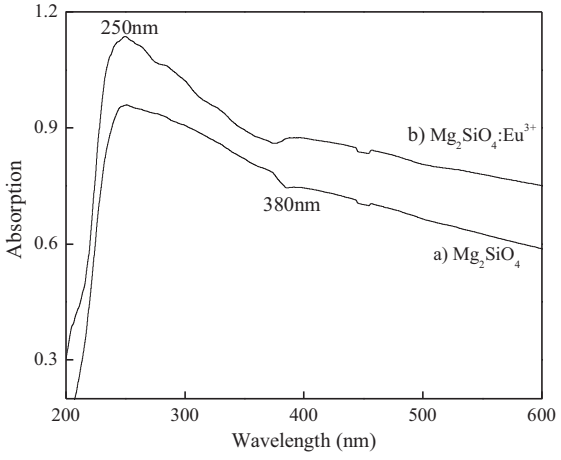

Fig. 3. Optical absorption spectra of (a) pure and (b) Eu^{3+} doped Mg_2SiO_4.

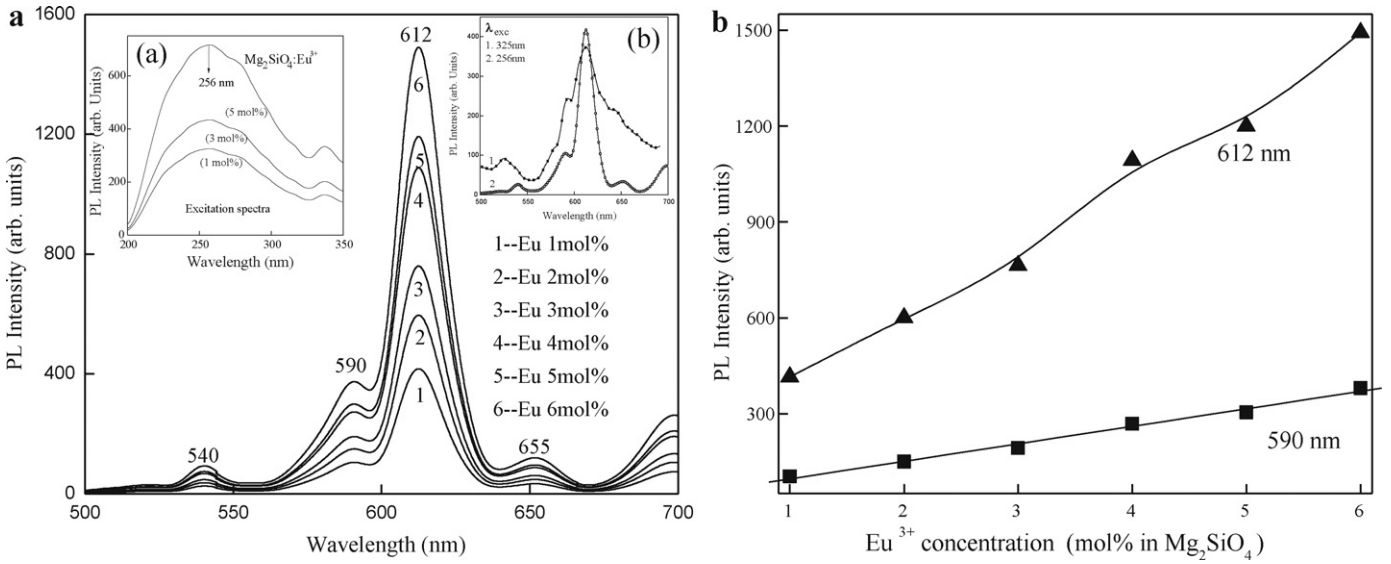

Fig. 4. (a) Emission spectra of Mg_2SiO_4:Eu^{3+}. Inset (a) excitation spectra (b) Comparison of emission spectra excited with 325 nm and 256 nm. (b) The effect of Eu^{3+} on the 590 nm and 612 nm emission peaks.

Mg_2SiO_4 is calculated using Tauc relation [15]. The energy gap of the Eu^{3+} (3 mol%) doped sample is found to be 5.84 eV.

The emission spectra of Mg_2SiO_4:Eu^{3+} (Inset a. excitation spectra b. comparison of emission spectra excited with 325 nm and 256 nm excitation) is shown in Fig. 4(a). The excitation spectrum consists of a charge transfer band (CTB) of Eu^{3+}–O^{2-} band in the short ultraviolet region (256 nm) [16]. The main factor affecting the intensity of the charge transfer band is the efficiency of the energy process from the CTB to the Eu^{3+} emitting level. It shows that with increasing heat treatment, the interaction between O^{2-} and Eu^{3+} ions in the silicate host becomes stronger which facilitates the electron transfer from O^{2-} to Eu^{3+} [17,18]. In the present study, the weak excitation peak observed at 337 nm suggests that the interaction between O^{2-} and Eu^{3+} is stronger; hence the efficiency of the energy transfer process from the charge transfer band (256 nm) to Eu^{3+} emitting levels increases. The f–f transitions within the Eu^{3+}, $4f^6$ configuration in longer spectral region with $^7F_0 \rightarrow {}^5D_3$ (337 nm) is the most prominent group [19].

A series of emission as shown in Fig. 4(a) with peaks at 540 nm, 590 nm, 612 nm, 655 nm may be attributed to the characteristic transitions of Eu^{3+} from $^5D_0 \rightarrow {}^7F_{j(j=0,1,2,3)}$. In particular, emission peak at 612 nm corresponds to $^5D_0 \rightarrow {}^7F_2$ and occurs through the forced electric dipole (FED), while the $^5D_0 \rightarrow {}^7F_1$ at 590 nm is the magnetic dipole transitions. The peak around 612 nm and 590 nm denote the Eu^{3+} ions occupy the Mg^{2+} sites with C2 or S6 symmetry. These two emissions are of particular interest because they represent actually the local environment of the Eu^{3+} ions. The $^5D_0 \rightarrow {}^7F_1$ is magnetic dipole allowed and its intensity shows variation with the crystal field strength surrounding the Eu^{3+} ions whereas, $^5D_0 \rightarrow {}^7F_2$ hypersensitive transition is electric dipole allowed and its intensity is sensitive to the local structure acting on the Eu^{3+} ion [19–23]. The Eu^{3+} ions enter into the host lattice and replace magnesium ion located on the surface of the nano crystals because of the porosity of Mg_2SiO_4. As dopant concentration of Eu^{3+} increases, $^5D_0 \rightarrow {}^7F_2$ transition dominates and the emission intensity increases. This may be attributed to the increase distortion of the local field around the Eu^{3+} ions [24,25]. The host material Mg_2SiO_4 is a member of the olivine family of crystals with orthorhombic crystalline structure in which Mg^{2+} occupies two nonequivalent octahedral sites: one (M1) with inversion symmetry (Ci) and the other (M2) with mirror symmetry (Cs) [8], When RE^{3+} ions doped into the host, they could probably occupy both sites. Based on this, Eu^{3+} is chosen to study luminescent properties of the material. The variation of PL intensity with europium mol concentration is shown in Fig. 4(b).

The Eu^{3+} energy level diagram corresponding to the $^5D_0 \rightarrow {}^7F_{j(j=0,1,2,3)}$ emission peaks is shown in Fig. 5. When the sample is excited by 256 nm wavelength, Eu^{3+} ion is raised to $^5L_6$ level from the ground state. Since, the separation between $^5D_0 \rightarrow {}^7F_{j(j=0,1,2,3)}$ is large, the stepwise decay process stops here and returns to ground state by giving emission in the orange and red regions. If the Eu^{3+} impurity does not occupy center of symmetry of the crystal lattice, then it will give both magnetic and electric dipole transitions. When the rare earth impurity ion is located at the center of symmetry in the relevant crystal lattice only magnetic dipole transition are allowed. The energy-level diagram indicates the states involved in the luminescence processes and the transition probabilities for Eu^{3+} ions. According to the model, the system is first excited from the ground state ($^5D_3$ configuration) to the singlet state of the $^5D_{3,2,1,0}$ configurations. Then the electrons

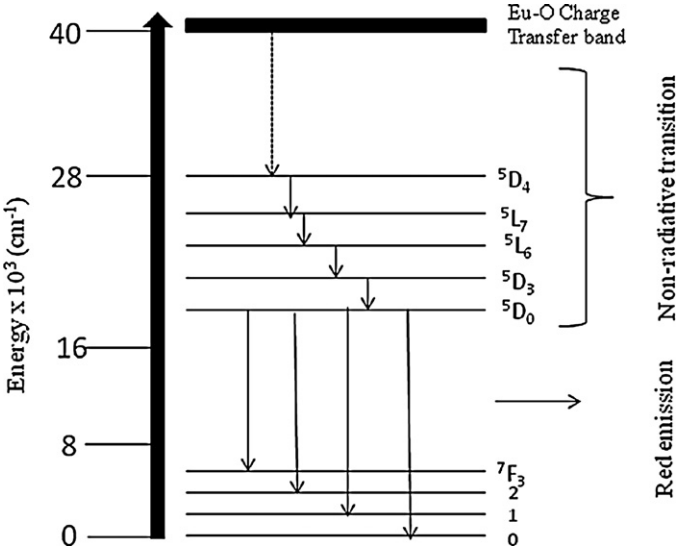

Fig. 5. The energy level diagram of Eu^{3+} ion showing the states involved in the luminescence process and the transition probabilities.

Table 1
Glow peak and kinetic parameters of the glow curve in Eu^{3+}doped Mg_2SiO_4.

Glow Peak temperature, T_m (°C)	Glow peak parameters				TL parameters		
	δ (°C)	τ (°C)	ω (°C)	μ_g	E_t (eV)	n_0 (cm^{-3})	S (s^{-1})
202	30	29	59	0.51	1.05	2.60×10^4	3.6×10^{10}
347	42	43	85	0.49	1.17	1.12×10^5	5.6×10^8

pass to the triplet state, mainly to level 4 because of symmetry reasons. The last transition $^5D_0$ is so much faster than any other step of the luminescence process. It may be considered at once that the singlet state does not affect the luminescent process. Non-radiative transitions occur between the third energy levels of the triplet state, named $^5D_3$, $^5D_2$, $^5D_1$ and $^5D_0$ with probabilities from level 3 to level 2, level 2 to level 1, and level 1 to level 0, i.e., $^5D_0$. Level $^5D_0$ to level $^7F_{0,1,2,3}$ occurs radiative transitions to the ground state, i.e., $^5D_0 \rightarrow {}^7F_j$ states respectively. The increase in PL intensity observed might be due to the decrease of cross relaxation between Eu^{3+} ions in this process [26].

Eu^{3+} ion in Mg_2SiO_4 prepared by combustion synthesis is situated at the low symmetry sites. In doped Mg_2SiO_4:Eu^{3+} ion enters into Mg^{2+} lattice site. The ionic radii of Eu^{3+} and Mg^{2+} are 0.095 and 0.072 nm respectively. Since ionic radius of Mg^{2+} is smaller than Eu^{3+}, Mg_2SiO_4 host could accommodate only small percentage of impurity ions. Moreover, there is charge imbalance in the host lattice due to doping of trivalent Eu^{3+} cations. This may absorb emitted light, resulting in to decrease of intensity. It is shown that relative intensity of the emission lines of Eu^{3+} depends on the doping concentration of Eu^{3+} in Mg_2SiO_4 phosphor. By increasing the Eu^{3+} concentration the transition $^5D_0 \rightarrow {}^7F_2$ (612 nm) has shown an enhanced emission.

Fig. 6 shows the thermoluminescence glow curves of Eu^{3+} doped magnesium silicate γ-rayed for 4.658 kGy. The glow curves clearly show two well resolved and well separated glows with peaks around 202 °C (T_{g1}) and 345 °C (T_{g2}) besides a shoulder with peak at around 240 °C. The glow peak temperature of T_{g1} and T_{g2} are almost steady for the entire dose range with increase of Eu^{3+} [27]. The peak around 202 °C is due to recombination of charges released from F^+ center near Mg^{2+}/Eu^{3+} sites [28] and peak around 345 °C may tentatively be attributed to recombination of F center electrons with holes associated with SiO_4 and Mg^{2+} sites. The electrons and holes formed in the phosphor during irradiation. During this time, the electrons were trapped in H^+ ion, resulting in a hydrogen atom center. The holes however, might become free. TL peak temperature depends on the activation energy (trap depth) required to release

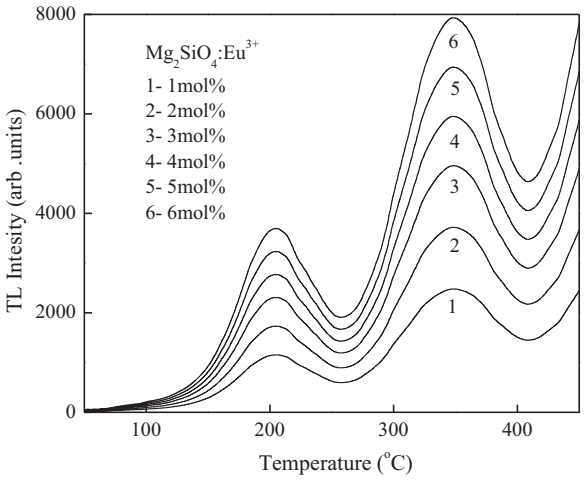

Fig. 6. TL glow curve of 4.658 kGy γ-rayed Mg_2SiO_4:Eu^{3+}.

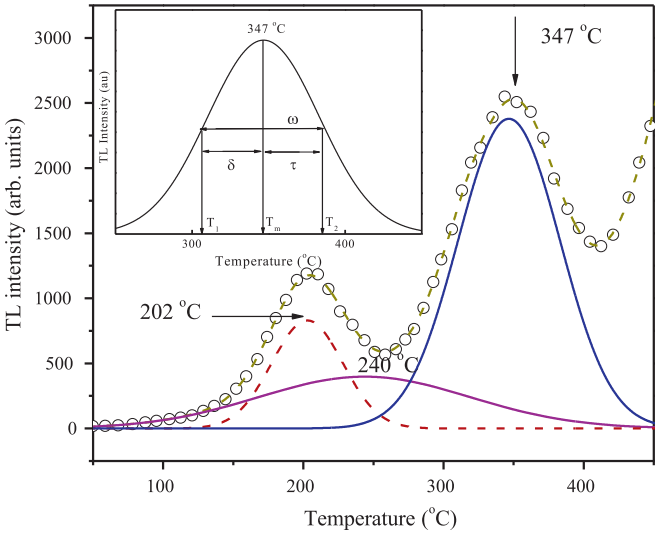

Fig. 7. TL deconvoluted curve of Mg_2SiO_4:Eu^{3+}.

the electrons from the hydrogen atom center. When phosphor is heated these electrons recombine with holes. Eu^{3+} ion was excited by the energy liberated on recombination between the released electron and the free hole, resulting in Thermoluminescence due to f → f transitions of Eu^{3+} ion. This doublet splitting is attributed to the ^1H of a nuclear spin $I = 1/2$. The TL emission peaks assigned to f → f transitions of Eu^{3+} ion which were found to be same as PL behavior of the phosphor [29,30]. The kinetic parameters are calculated based on glow curve shape method (modified by Chen) using computerized glow curve deconvolution [31,32] and are shown in Fig. 7 and results are tabulated in Table 1. The dominant trapping centers of a phosphor with trap depths in the range 1.0–1.2 eV show excellent phosphorescence property and it may be responsible for enhanced afterglow emission [33].

4. Conclusions

Mg_2SiO_4 doped with different mol concentrations of europium nanocrystalline phosphor is prepared at ~800 °C and in a very short time (<5 min) using solution combustion technique. The PXRD pattern showed the alpha phase, orthorhombic structure of the samples and the particle size is observed in the nano scale. The UV–vis absorption of pure and doped phosphor show an intense absorption band in the region 240–270 nm corresponding to oxygen to silicon (O–Si) ligand-to-metal charge-transfer (LMCT) in the SiO_3^{2-} group. The phosphor exhibits different emission (in the range 540–660 nm) due to Eu^{3+} corresponding to $^5D_0 \rightarrow {}^7F_{j(j=0,1,2,3)}$ transitions. The transition centered at 612 nm is found to be hypersensitive in nature resulting in a strong and red emission. Enhancement in PL intensity of Eu^{3+} was observed due to the formation of different lattice sites in the host phosphor. The PL behavior is supported by the TL characteristics. In the present work, Mg_2SiO_4 doped with Eu^{3+} are investigated as new red phosphor with good emission color purity due to the non-centrosymmetric site for the

europium ion. Further, the excellent emission properties of this phosphor suggest that it may be used for display applications.

References

[1] W. Ganngam Phaomei, R.S. Rameshwor Singh, Ningthoujam, J. Lumin. 131 (2011) 1164.
[2] Feng Zhang, Yuhua Wang, Yan Wen, Dan Wang, Ye Tao, Opt. Mater. 33 (2011) 475.
[3] H. Shabir, B. Lal, M. Rafat, J. Sol-Gel Sci. Technol. 53 (2010) 399.
[4] S. Cho, R. Lee, H. Lee, J. Kim, C. Moon, S. Nam, J. Park, J. Sol-Gel Sci. Technol. 53 (2010) 171.
[5] Juan Wang, Yunhua Xu, Mirrabos Hojamberdiev, Jianhong Peng, Gangqiang Zhu, J. Non-Cryst. Solid 355 (2009) 903.
[6] E.M. Yoshimura, E.G. Yukhihara, NIM-B 250 (2006) 337.
[7] Numan Salah, Sami S. Habib, Zishan H. Khan, Salim Al-Hamedi, S.P. Lochab, J. Lumin. 129 (2009) 192.
[8] Hongmei Yang, Jianxin Shi, Menglian Gong, K.W. Cheah, J. Lumin. 118 (2006) 257.
[9] S. Ekambaram, K.C. Patil, J. Mater. Chem. 5 (1995) 905.
[10] R. Tenne, Chem. Eur. J. 8 (2002) 5297.
[11] J.T. Hu, T.W. Odom, C.M. Lieber, Acc. Chem. Res. 32 (1999) 435.
[12] M.T. Tsai, Mater. Res. Bull. 37 (2002) 2213.
[13] G.A. Kumar, C.W. Chen, J. Ballato, R.E. Riman, Chem. Mater. 19 (2007) 1523.
[14] S. Atalay, H.I. Adiguzel, F. Atalay, Mater. Sci. Eng. A 304 (2001) 796.
[15] J. Tauc, R. Grigorovici, A. Vancu, Opt. Phys. Status Solidi 15 (1966) 627.
[16] Qingguo Meng, Jun Lin, Lianshe Fu, Zhang Hongjie, Wang Shubin, Yonghui Zhou, J. Mater. Chem. 11 (2001) 3382.
[17] X.P. Fan, M.Q. Wang, Z.L. Hong, G.D. Qian, J. Phys.: Condens. Matter 9 (1997) 3479.
[18] C. Louis, R. Bazzi Marco, A. Flores, W. Zheng, K. Lebbou, O. Tillement, B. Mercier, C. Dujardin, P. Perriat, J. Solid State Chem. 173 (2003) 335.
[19] Mao Shengping, Liu Qun, Gu Meng, Mao Dali, Chang Chengkang, J. Alloys Compd. 465 (2008) 367.
[20] J. Trojan Piegza, E. Zych, D. Hreniak, W. Strek, L. Kepenski, J. Phys.: Condens. Matter 16 (2004) 6983.
[21] G. Concas, G. Spano, E. Zych, T. Trojan, J. Phys.: Condens. Matter 17 (2005) 2597.
[22] R. Krsmanovi, O.I. Lebedev, A. Speghini, M. Bettinelli, S. Pollizzi, Van Tendello, Nanotechnology 17 (2006) 2805.
[23] Xiang Ying Chen, Chao Ma, Zhong Jie Zhang, Xiao Xuan Li, Microporous Mesoporous Mater. 123 (2009) 202.
[24] Vu Nguyen, Tran kim Anh, Gyu-chul Yi, W. Trek, J. Lumin. 122 (2007) 776.
[25] Viagin Oleg, Masalov Andrey, Ganina Irina, Malyukin Yuriy, Opt. Mater. 31 (2009) 1808.
[26] I.M. Nagpure, Subhajit Saha, S.J. Dhoble, J. Lumin. 129 (2009) 898.
[27] E.G. Yikihara, R. Gaza, S.W.S. McKeever, C.G. Soares, Radiat. Meas. 38 (2004) 59.
[28] T.K. Vijay Singh, Gundu Rao, Jun-Jie Zhu, J. Lumin. 126 (2007) 1.
[29] K. Nakashima, M. Takami, M. Ohta, T. Yasue, J. yamauchi, J. Lumin. 111 (2005) 113.
[30] I.M. Nagpure, S. Saha, S.J. Dhoble, J. Lumin. 129 (2009) 898.
[31] N. Suriyamurthy, B.S. Panigrahi, J. Lumin. 128 (2008) 1809.
[32] R. Chen, J. Electrochem. Soc. 116 (1969) 1254.
[33] T. Katsumata, R. Sakai, S. Komuro, T. Morikawa, J. Electrochem. Soc. 150 (2003) H111.